Pole/Zero Design of Agonist/Antagonist Actuation

Patrick J. Schimoler, *Member, IEEE*, Jeffrey S. Vipperman, *Member, IEEE*, and Mark Carl Miller

***Abstract*— Objective: This brief analyzes the open-loop dynamics of coupled (dedicated) and decoupled tendon tension control methods in an agonist/antagonist (AA) actuator pair, a fundamental control unit used in orthopedic testbeds known as joint motion simulators (JMSs). Methods: A linear mathematical model of an AA actuator pair is derived. Transfer functions from tendon tension control signal to tendon tension and joint position are derived. Sources of key dynamics are explained. Results: The system's dynamic model shows that both the dedicated and decoupled approaches have a low-frequency pole pair, a low-frequency zero pair, and a mid-range zero pair. A frequency domain identification of the flexion/extension axis of an existing elbow JMS validates the locations of these dynamics. The interaction between tendon tension control and joint position is shown to be controllable in decoupled control, but not in dedicated control. The bandwidth reduction due to the low-frequency pole pair and low-frequency zero pair are shown to be controllable in decoupled control, but not in dedicated control. Conclusion: Decoupled control is superior to dedicated control for AA actuator pairs in JMS designs because it reduces actuator interaction and has a larger tension control bandwidth. Significance: This analysis describes the sources of the dynamics seen in the open-loop frequency response of both methods and shows the superiority of the decoupled method in tension control bandwidth and in lack of interactions with position control.**

***Index Terms*— Agonist/antagonist (AA) actuation, decoupled feedback control, force control, joint motion simulator (JMS), tendon actuation.**

I. Introduction

THE joints of the human body enable a person to move and interact with their environment. Research on joint function, injury, and repair is critical for maintaining and extending a person's quality of life. *In vitro* cadaveric testing enables many methods impossible *in vivo*, such as invasive instrumentation of tissues, application of multiple surgical techniques to the same specimen, and testing of various states of injury. While cadaveric joint testing removes the restrictions of *in vivo* testing, the absence of the central nervous system to actuate the muscles around the joint necessitates the development of external means to move a joint in a way that will yield meaningful data. One of these external means is the joint motion simulator (JMS).

Manuscript received November 11, 2016; revised June 22, 2017; accepted July 20, 2017. Manuscript received in final form August 11, 2017. Recommended by Associate Editor A. Behal. *(Corresponding author: Patrick J. Schimoler.)*

P. J. Schimoler and M. C. Miller are with the Mechanical Engineering and Materials Science Department, University of Pittsburgh, Pittsburgh, PA 15213 USA, and also with the Orthopedic Surgery Department, Allegheny General Hospital, Pittsburgh, PA 15212 USA (e-mail: pjs50@pitt.edu).

J. S. Vipperman is with the Mechanical Engineering and Materials Science and Bioengineering Department, University of Pittsburgh, Pittsburgh, PA 15213 USA.

Color versions of one or more of the figures in this paper are available online at http://ieeexplore.ieee.org.

Digital Object Identifier 10.1109/TCST.2017.2740852

JMSs are tendon actuated, computer controlled devices built for research on cadaveric joints. A frame, pulley system, tension and position sensors, motors, controller, and cadaveric specimen comprise a typical JMS. The frame rigidly holds one side of the specimen and supports the motors. A controller drives motors generating forces applied to the exposed tendinous insertions of the freely moving side of the specimen. A pulley system, also mounted on the frame, guides cables along physiologic lines of action while sensors measure tendon tensions and joint positions. Tendon actuation generates joint loading and motion that are as physiologic as possible and computer control reduces the variability in testing compared to manual actuation [1]. Tendon actuation and computer control ensure that collected data represents *in vivo* joint behavior. JMSs have been developed for many joints: elbows [2]–[4], wrists/hands [5], [6], shoulders [7]–[11], feet/ankles [12]–[17], and knees [18]–[22]. JMS experiments often entail tracking prescribed joint angle profiles, applying prescribed tendon tension profiles, or combinations of both.

The unidirectional nature of tendon actuation complicates JMS control. Tendon slack may occur, creating three problems: nonlinear behavior, lack of control in the slack direction, and motion delayed until slack is removed. The choice of the muscles simulated by the actuators can help prevent slack. For each actuated muscle, the JMS can include another with an opposing moment about the joint. The human body effectively uses these agonist/antagonist (AA) pairings. Co-contraction in AA pairs of simulated muscles prevents tendon slack. Even if joint position and not joint loading is the primary purpose of a JMS experiment, the control scheme can effectively include positive cable tension to prevent tendon slack, which would degrade joint position control.

Various control methods have been applied to JMSs to manage tendon actuation and apply physiologic loading. One common method dedicated one actuator per degree of freedom (DOF) to control joint position and the remaining actuators to control tendon tension [2]. This technique ensured tension in the actuator responsible for joint position control allowing motion in both directions. Previous researchers advanced this approach with one actuator dedicated to one control task with load profiles determined from electromyographic (EMG) experiments [9], with libraries of human subject data to manage specimen variation [23], or with logic sets enabling motion in various planes [24].

Before its use in JMS control, dedicated actuator assignment appeared in tendon-driven robotics for AA pairings [25]. Other AA control approaches within robotics spread individual control responsibilities among multiple actuators controlling joint position and stiffness [26] and joint torque and stiffness [27]. Advanced forms of this control method switched actuator roles as necessary to minimize opposing actuator tension

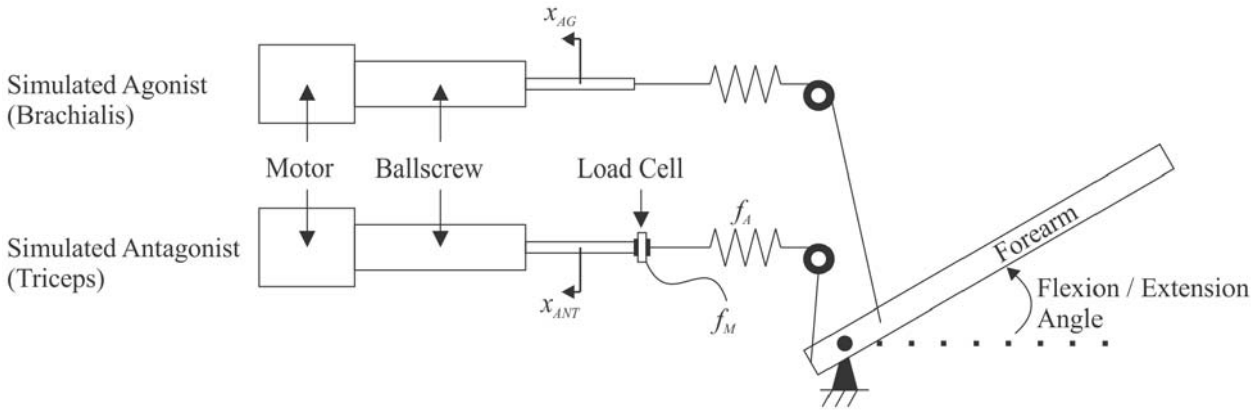

Fig. 1. Nonlinear elbow FE model with single AA actuator pair and antagonist load cell. In this simple elbow model, the triceps act as an antagonist and the brachialis as an agonist.

while still controlling joint position [28]. The distribution of a given control responsibility among multiple actuators reduced interactions between control tasks.

As the existing approaches have shown, the responsibility for the control of one kinematic DOF or one muscle's tendon tension may be either assigned to one dedicated actuator or spread among multiple actuators. The first method, called in this brief a dedicated control design, assigns one actuator to one control responsibility at any given time. A dedicated actuator has a single control responsibility. The second method, denominated in this brief as a decoupled control design, assigns a combination of actuators to a given responsibility at any given time. The decoupled approach requires an actuator to have multiple responsibilities although it shares each responsibility with other actuators.

The frequency domain dynamics of tendon-actuated AA systems expose their limitations and are therefore of importance to JMS designers and users. A joint's inertia and tendon stiffness combine to form low-frequency dynamics that limit JMS performance. Differences in the low-frequency dynamics between the dedicated and decoupled approaches provide the decoupled approach with a greater tension control bandwidth and less interaction with position control. Additionally, the usual in-series placement of a load cell between actuator and tendon creates higher frequency dynamics that limit the range of accurate tendon tension measurement in both methods of control.

The purpose of this brief is to describe these important dynamics present in only the tendon tension control aspect of AA JMS designs and to show that the proposed decoupled approach, despite its added complexity, is superior to the dedicated approach for JMS tendon tension control.

II. Mathematical Modeling of Agonist/Antagonist Pairing

The Allegheny General Hospital (AGH) elbow JMS uses the brachialis, biceps, pronator teres, and triceps to load the joint and move an elbow through flexion/extension (FE) and pronation/supination (PS) motions. The four muscles comprise a minimum set needed to actuate both kinematic DOFs. To clearly explain the dynamics of an AA actuator pair, this brief focuses on a single AA pair: the brachialis and triceps used to control elbow FE.

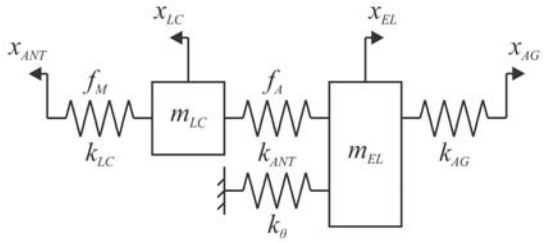

Fig. 2. Linear elbow FE model with single AA actuator pair.

The FE DOF (Fig. 1) is composed of cabling, the elbow itself, a load cell which measures the antagonist tension, springs and two velocity controlled motors connected to ball screws that convert the motors' rotary motion into linear motion. Over the bandwidth of interest, the motors act as ideal velocity sources so that actuator mass and stiffness are excluded. The antagonist load cell stiffness and mass, however, are included in the model to provide an antagonist tension output and to explain the source of dynamics discussed later. The load cell's stiffness is several orders of magnitude higher than all other stiffnesses in the system. The actual system also includes an agonist load cell, which is excluded in the current model, because it neither contributes any meaningful dynamics nor generates a sensor signal of interest.

Linearization of the elbow JMS model produces a two DOF spring-mass assembly (Fig. 2) governed by two differential equations as follows:

$$m_{\mathrm{EL}}\ddot{x}_{\mathrm{EL}} = -k_{\mathrm{ANT}}(x_{\mathrm{LC}}+x_{\mathrm{EL}})-k_\theta x_{\mathrm{EL}}+k_{\mathrm{AG}}(x_{\mathrm{AG}}-x_{\mathrm{EL}}) \quad (1)$$

$$m_{\mathrm{LC}}\ddot{x}_{\mathrm{LC}} = k_{\mathrm{LC}}(x_{\mathrm{ANT}} - x_{\mathrm{LC}}) - k_{\mathrm{ANT}}(x_{\mathrm{LC}} + x_{\mathrm{EL}}). \quad (2)$$

Positions for the elbow, load cell, antagonist input, and agonist input are represented by variables x_{EL}, x_{LC}, x_{ANT}, and x_{AG}, respectively. Tensions in the load cell and antagonist are represented by variables f_M and f_A, respectively. Load cell and elbow inertia are described by parameters m_{LC} and m_{EL}, respectively. Stiffnesses for the load cell, antagonist actuator, agonist actuator, and FE angle dependent moment arms are described by k_{LC}, k_{ANT}, k_{AG}, and k_θ, respectively. In the underlying nonlinear system, changes in FE angle can also change the tendons' angles of attack varying net moments

even if tendon tensions are unchanged; this effect yields the moment arm stiffness during linearization. The frequency domain analysis of this linear spring-mass model illustrates the dynamics of the elbow JMS's AA pairing.

A. Single Actuator Assignment

One approach to controlling a single DOF AA pair is termed "dedicated actuator assignment" or "dedicated control." Within a pair of actuators, one actuator is responsible for tendon tension control and the other actuator is responsible for joint position control. In performing its designated task without consideration of the other actuator's task, each actuator generates a disturbance to the other control task. From a tension control perspective, the agonist actuator is unused (3), so that (1) can be simplified to (4)

$$x_{\mathrm{AG}} = 0 \tag{3}$$

$$m_{\mathrm{EL}}\ddot{x}_{\mathrm{EL}} = -k_{\mathrm{ANT}}(x_{\mathrm{LC}} + x_{\mathrm{EL}}) - k_\theta x_{\mathrm{EL}} - k_{\mathrm{AG}} x_{\mathrm{EL}}. \tag{4}$$

B. Dual Actuator Assignments

Another approach to controlling a single DOF AA pair is termed "decoupled actuator assignment" or "decoupled control." Decoupled feedback control, a common multivariable control technique [29], spreads the task of reducing a joint position error or tendon tension error across both actuators. Decoupled feedback control results in an agonist and antagonist that move in some proportion to each other in response to joint position or tendon tension errors. Were it not for k_θ, the AA actuators, x_{ANT} and x_{AG}, could change joint position without affecting tendon tension by simply moving together maintaining a constant displacement from each other. With k_θ present, x_{AG}'s motion must be the sum of two parts: one part matching the motions of x_{ANT} and a second part balancing the tension in k_θ. For tendon tension control, the AA actuators move apart from each other in an assigned proportion (5). This movement maintains the net moment on the elbow, preventing a change in motion, while increasing or decreasing the antagonist tendon tension. Equation (5) simplifies (1) into (6)

$$x_{\mathrm{AG}} = \alpha x_{\mathrm{ANT}} \tag{5}$$

$$m_{\mathrm{EL}}\ddot{x}_{\mathrm{EL}} = -k_{\mathrm{ANT}}(x_{\mathrm{LC}} + x_{\mathrm{EL}}) - k_\theta x_{\mathrm{EL}} + k_{\mathrm{AG}}(\alpha x_{\mathrm{ANT}} - x_{\mathrm{EL}}). \tag{6}$$

The decoupling gain α is chosen through consideration of the system's stiffnesses and moment arms so that reduction in tendon tension error is possible without negatively affecting joint position control. A constant gain decouples tendon tension control from joint position at low frequencies where the system's gain is closely approximated by the system's dc gain. This gain is only a portion of a fully decoupled approach that also decouples joint position control from tendon tension control. With this constant gain, either the AA pair can be decoupled around the value of the angle at which the system is linearized or the decoupling gain can be chosen as a function of elbow orientation.

Although both actuators are responsible for tension control in the decoupled approach, designated agonist and antagonist remain because the control loop still requires a measure of tendon tension for closure. It is assumed here that the tension in the antagonist closes the tension control loop. This tension source can be switched as a function of system states to the benefit of the system's performance [30].

III. Transfer Functions and Their Approximations

The relevant transfer functions of the dedicated and of the decoupled tension control approaches result from application of Cramer's Rule to the system's transfer function matrix (7), which also yields the characteristic equation (8)

$$\begin{bmatrix} m_{\mathrm{LC}}s^2 & 0 & -1 & 1 \\ 0 & m_{\mathrm{EL}}s^2 + k_{\mathrm{AG}} + k_\theta & 0 & 1 \\ k_{\mathrm{LC}} & 0 & 1 & 0 \\ -k_{\mathrm{ANT}} & -k_{\mathrm{ANT}} & 0 & 1 \end{bmatrix} \begin{Bmatrix} X_{\mathrm{LC}} \\ X_{\mathrm{EL}} \\ F_M \\ F_A \end{Bmatrix} = \begin{bmatrix} 0 & 0 \\ 0 & \dfrac{k_{\mathrm{AG}}}{s} \\ \dfrac{k_{\mathrm{LC}}}{s} & 0 \\ 0 & 0 \end{bmatrix} \begin{bmatrix} 1 \\ \alpha \end{bmatrix} \{U_F\} \tag{7}$$

$$\Delta = \left(m_{\mathrm{LC}}s^2 + k_{\mathrm{LC}}\right)\left(m_{\mathrm{EL}}s^2 + k_{\mathrm{ANT}} + k_{\mathrm{AG}} + k_\theta\right) + k_{\mathrm{ANT}}\left(m_{\mathrm{EL}}s^2 + k_{\mathrm{AG}} + k_\theta\right). \tag{8}$$

The three transfer functions of interest are: 1) tension control signal U_F to measured tension, F_M (9); 2) tension control signal U_F to applied tension, F_A (10); and 3) tension control signal U_F to antagonist insertion position, X_{EL} (11)

$$\frac{F_M}{U_F} = k_{\mathrm{LC}}\left[m_{\mathrm{LC}}s^2\left(m_{\mathrm{EL}}s^2 + k_{\mathrm{ANT}} + k_{\mathrm{AG}} + k_\theta\right) + k_{\mathrm{ANT}}\left(m_{\mathrm{EL}}s^2 + (1+\alpha)k_{\mathrm{AG}} + k_\theta\right)\right]/(s\Delta) \tag{9}$$

$$\frac{F_A}{U_F} = \left[k_{\mathrm{LC}}k_{\mathrm{ANT}}\left(m_{\mathrm{EL}}s^2 + (1+\alpha)k_{\mathrm{AG}} + k_\theta\right) + \alpha k_{ANT}k_{AG}m_{LC}s^2\right]/(s\Delta) \tag{10}$$

$$\frac{X_{\mathrm{EL}}}{U_F} = \left[\alpha k_{\mathrm{AG}}\left(m_{\mathrm{LC}}s^2 + k_{\mathrm{LC}} + k_{\mathrm{ANT}}\right) - k_{\mathrm{LC}}k_{\mathrm{ANT}}\right]/(s\Delta). \tag{11}$$

The tension control signal originates from a tension controller connected to a comparator outputting tension error. Dedicated control can be viewed as a limiting case of decoupled control in which the decoupling gain α in (5) is zero, thereby reducing the necessary number of transfer functions.

All three transfer functions (9)–(11) share the same characteristic equation and poles, assuming no pole-zero cancellations. JMS's operate in frequency ranges below those in which the load cell's inertial effects become important. This frequency restriction and a load cell's high relative stiffness (12) simplify (8) into (13) showing that the low-frequency pole pair is approximated by the natural frequency ω_{LFP} (14) of a subsystem [Fig. 3(a)] of the AA pair

$$k_{\mathrm{LC}} \gg m_{\mathrm{LC}}s^2, k_{\mathrm{ANT}} \tag{12}$$

$$\Delta \approx k_{\mathrm{LC}}\left(m_{\mathrm{EL}}s^2 + k_{\mathrm{ANT}} + k_{\mathrm{AG}} + k_\theta\right) \tag{13}$$

$$\omega_{\mathrm{LFP}} = \sqrt{\frac{k_{\mathrm{ANT}} + k_{\mathrm{AG}} + k_\theta}{m_{\mathrm{EL}}}}. \tag{14}$$

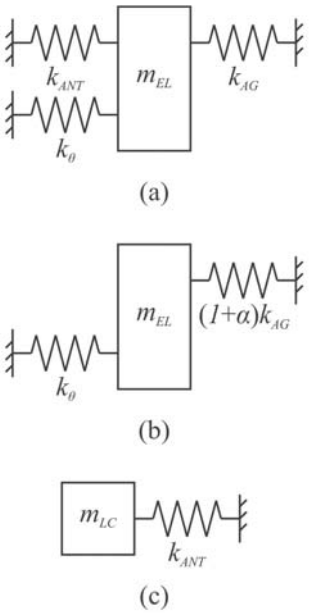

Fig. 3. Subsystems whose natural frequencies describe the locations of the FE AA pair's dynamics of interest. (a) Low-frequency pole. (b) Low-frequency zero. (c) Mid-range zero.

The tension control to measured tension (9) and from tension control to applied tension (10) transfer functions share the same zero pair which is located at the natural frequency ω_{LFZ} (15) of the subsystem containing the elbow mass, moment arm stiffness, and the agonist stiffness scaled by the decoupling gain plus one [Fig. 3(b)]. The approximate location of the zero pair can be made evident from (9) by simplifying the numerator to (16), because the antagonist stiffness dominates the load cell's inertial effects (17) at low frequencies. Similarly, the zero pair can be made evident from (10) by simplifying the numerator to (16) because the load cell's stiffness dominates, at low frequencies, the inertial effects of the load cell as scaled by the decoupling gain and the linearized agonist stiffness (18)

$$\omega_{\mathrm{LFZ}} = \sqrt{\frac{(\alpha+1)k_{\mathrm{AG}} + k_\theta}{m_{\mathrm{EL}}}} \tag{15}$$

$$\mathrm{Num}\left(\frac{F_M}{U_F}\right), \mathrm{Num}\left(\frac{F_A}{U_F}\right) \approx k_{\mathrm{LC}}k_{\mathrm{ANT}}\left(m_{\mathrm{EL}}s^2 + (1+\alpha)k_{\mathrm{AG}} + k_\theta\right) \tag{16}$$

$$k_{\mathrm{ANT}} \gg m_{\mathrm{LC}}s^2 \tag{17}$$

$$k_{\mathrm{LC}} \gg \alpha k_{\mathrm{AG}} m_{\mathrm{LC}}s^2. \tag{18}$$

The transfer function from tension control to measured tension has an additional zero pair in the frequency range where the elbow's inertial effects dominate the effects of the system's stiffnesses, not including the load cell stiffness (19). Inequality (19) simplifies the numerator of (9) to (20), showing that the zero pair's location is approximated by the natural frequency ω_{MRZ} (21) of the subsystem containing the antagonist stiffness and the load cell mass [Fig. 3(c)]

TABLE I
SIMULATION PARAMETERS

Symbol	Quantity	Value
k_{AG}	agonist stiffness	1.37×10^4 N/m
k_{ANT}	antagonist stiffness	8.59×10^3 N/m
k_{LC}	load cell stiffness	1.00×10^7 N/m
k_θ	moment arm stiffness	8.19×10^3 N/m
m_{EL}	elbow mass	5.68 kg
m_{LC}	load cell mass	4.64×10^{-2} kg

$$m_{\mathrm{EL}}s^2 \gg k_{\mathrm{ANT}}, k_{\mathrm{AG}}, k_\theta \tag{19}$$

$$\mathrm{Num}\left(\frac{F_M}{U_F}\right) \approx k_{\mathrm{LC}}m_{\mathrm{EL}}s^2\left(m_{\mathrm{LC}}s^2 + k_{\mathrm{ANT}}\right) \tag{20}$$

$$\omega_{\mathrm{MRZ}} = \sqrt{\frac{k_{\mathrm{ANT}}}{m_{\mathrm{LC}}}}. \tag{21}$$

The numerator of the transfer function from tension control signal U_F to elbow position X_{EL} (11) can be simplified, due to the large load cell stiffness relative to the load cell's inertia at low frequencies and to the system's other stiffnesses (22), to (23). Equation (23) shows the potential for decoupling tension control from joint position over low frequencies through the tuning of α

$$k_{\mathrm{LC}} \gg m_{\mathrm{LC}}s^2, k_{\mathrm{ANT}} \tag{22}$$

$$\mathrm{Num}\left(\frac{X_{\mathrm{EL}}}{U_F}\right) \approx k_{\mathrm{LC}}(\alpha k_{\mathrm{AG}} - k_{\mathrm{ANT}}). \tag{23}$$

Simple, system parameter combinations approximate frequencies of a low-frequency pole pair (14), low-frequency zero pair (15), and mid-range zero pair (21) of both the dedicated and decoupled systems.

IV. Model Validation

The dedicated and decoupled models were demonstrated and validated on the AGH elbow JMS [4]. The experimental frequency responses were found through a stepped-sine identification applied to a mechanical elbow. The parameters populating the model are listed in Table I. The mechanical elbow's inertia was determined through its swinging period and its damping ratio was calculated through the log decrement of its free response. The load cell mass and individual muscle (actuator) stiffnesses were found through individual identification procedures with the insertion end of the tendon (cable) connected to a rigid support instead of the elbow. Although ideal decoupling was calculated to be 0.625, the decoupling constant was set to 1.5. This exacerbated the effects of the low-frequency pole and low-frequency zero, making the models' match or mismatch more evident. The system was excited with frequencies between 1 and 80 Hz.

A direct comparison of the experimental identification to the theoretical values in the transfer function magnitude of tension control to measured tension (Figs. 4 and 5) validated the analysis. The frequencies (14, 15, and 21) of the pole and

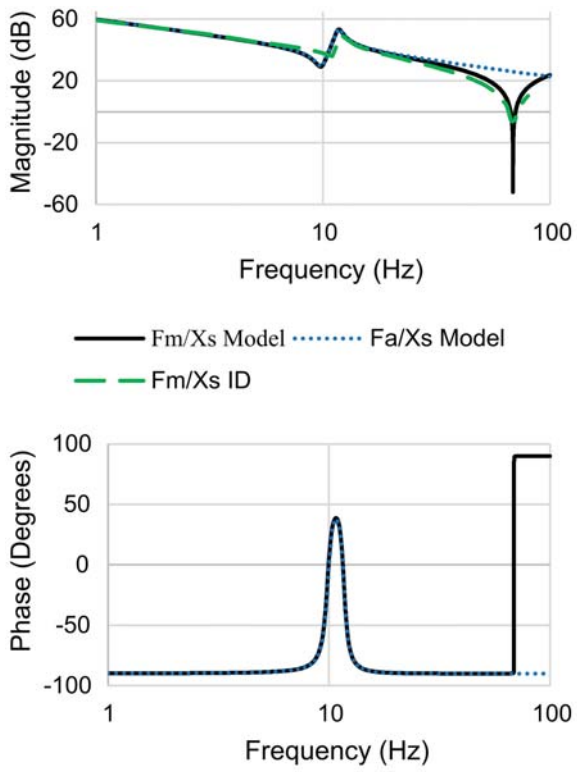

Fig. 4. Dedicated control tendon tension frequency response. The model agrees well with the experimentally identified location of the poles and zeros, but underestimates the amount of damping. The model did not include any damping of the mid-range zero.

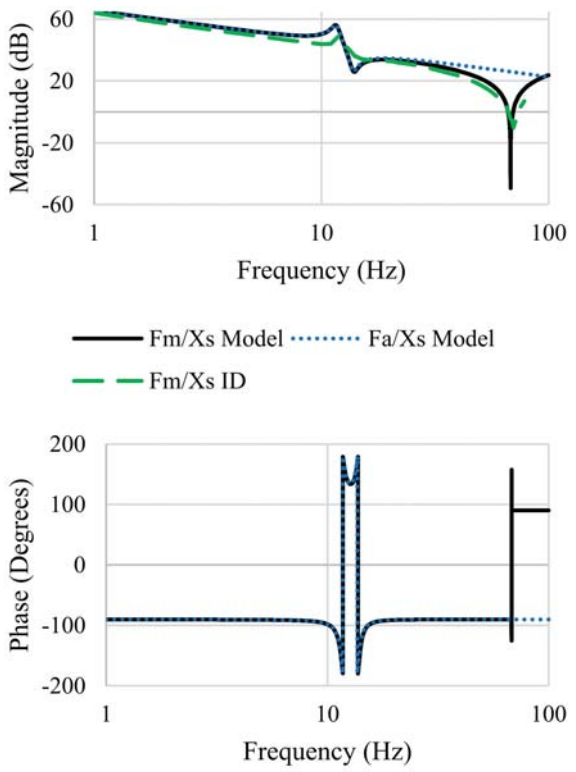

Fig. 5. Decoupled control tendon tension frequency response. Again, the model agrees well with the experimentally identified location of the poles and zeros, but underestimates the damping. The model did not include any damping of the mid-range zero.

zeros were reproduced very well, although the experimental system showed greater damping than predicted. In both cases the greatest error in predication was at the low-frequency zero, which the model underestimated in the dedicated case by approximately 1.2 Hz (11.2%) and in the decoupled case by approximately 1 Hz (6.9%).

V. Discussion

This brief compared dedicated and decoupled actuator assignment, two methods for performing tendon tension control and joint position control on an AA actuator pairing. Three open-loop transfer functions arising in the comparison of the two control methods of tendon tension were derived, simulated, identified, and compared: first, tension control signal to measured antagonist tension (9), second, tension control signal to applied antagonist tension (10), and, third, tension control signal to antagonist insertion position (11). The last transfer function was proportional to elbow position and indicated the amount of coupling between tension control and elbow position. A frequency response analysis showed that both methods have a low-frequency pole pair, a low-frequency zero pair, and a mid-range zero pair. The load cell's poles were omitted from the analysis because their high frequency precluded them from effecting system behavior.

The low-frequency pole pair appeared at the same frequency in all three open-loop transfer functions for both dedicated and decoupled control. Its frequency was dictated by the elbow's mass and the antagonist stiffness, agonist stiffness, and moment arm stiffness. This restoring stiffness was a function of elbow angle and depended on the operating point about which linearization took place.

Theoretically, perfect decoupling would have completely hidden this pole pair in the decoupled tension control equations because the agonist and antagonist would apply equal moments to both sides of the elbow, varying the antagonist tension without changing the elbow's position. Uncertainty in stiffnesses, moment arms, and a dependence on elbow position made perfect decoupling unrealistic. However, the model showed that even reasonably good decoupling would have significantly reduced the pole pair's effect by bringing the low-frequency zero pair into closer proximity of the pole pair, where their effects would offset extending the tension control bandwidth by making the frequency response more like that of the ideal velocity source connected to a stiffness alone (Fig. 6).

The low-frequency zero pair appeared in both the measured and applied tension transfer functions for both the dedicated and decoupled approaches. This zero pair was fundamentally limiting because it appeared in the applied tendon tension transfer function: the goal of tension control, to apply a commanded tension, was diminished at these frequencies.

The low-frequency zero pair's location depended on the choice of dedicated or decoupled actuation. The decoupled approach benefits were clear: the frequency at which this zero pair appeared (15) was higher in the decoupled case than in the dedicated case and the decoupled case could reduce the effect of the zero pair on the frequency response as a function of the quality of the decoupling. Thus, the decoupled tension control had the potential for a greater bandwidth than

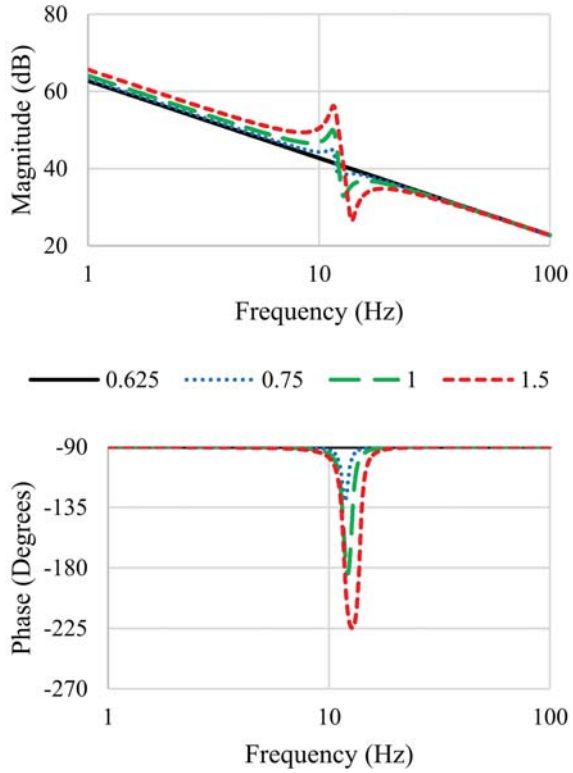

Fig. 6. Tension control to applied tension for a decoupled system as a function of different decoupling gains. For the given system, perfect decoupling of tendon tension control from joint position occurs for a decoupling gain of approximately 0.625. As decoupling gains approach this ideal value from above, from below would be true as well, the effects of the low-frequency pole offset the effects of the low-frequency zero. For reasonably good cancellation, the tension control bandwidth is extended beyond that of the dedicated controller.

dedicated control. Accurate tuning of the decoupling gain could put the low-frequency pole pair and low-frequency zero pair in close proximity, nearly canceling their effects and extending the tension control bandwidth (Fig. 6).

In the dedicated control case, the low-frequency zero pair's location was approximated by the natural frequency of a subsystem consisting of the elbow inertia, linearized agonist stiffness, and linearized rotational stiffness (15 with $\alpha = 0$). When the antagonist actuator was driven at the subsystem's natural frequency, the ideal subsystem had zero impedance. No supply of energy, beyond the small amount dissipated by the damping, was needed to excite or maintain oscillations at this frequency, meaning that no application of force to the mass was needed. This absence of force because of the subsystem's zero impedance manifested itself as a zero in the applied tension transfer function. The measured tension transfer function had a similar zero. If no force transmission through the agonist stiffness was needed to make the system move with the actuator, then no force need be transmitted through the load cell at that frequency either.

In the decoupled control case, the low-frequency zero pair's location was approximated by the natural frequency of a subsystem composed of the elbow inertia, the linearized agonist stiffness scaled by one plus the decoupling gain, and the moment arm stiffness. A frequency difference of this zero pair between the dedicated and decoupled control cases arose because of motion of the agonist actuator in the decoupled case. The same zero impedance argument explains why no force was transmitted across the load cell or antagonist stiffness in the undamped case: no force was necessary to keep the subsystem moving in phase with the antagonist actuator when the antagonist actuator was driven at the natural frequency of the subsystem. Because the elbow mass and antagonist actuator were in phase and the antagonist actuator and the agonist actuator were controlled to be 180° out of phase, the agonist actuator and the elbow mass were necessarily 180° out of phase. Additionally, because the elbow mass and antagonist actuator had the same motion magnitude and the antagonist actuator and agonist actuator had motion magnitudes related by the decoupling gain, the agonist actuator and elbow mass also had magnitudes related by the decoupling gain, α. The 180° phase difference with a fixed magnitude relationship between the agonist actuator and elbow mass effectively put a node into the agonist stiffness, dividing it into two parts. The part of the stiffness on the mass side of the node translated in the same direction as the mass, while the part of the stiffness on the actuator side translated in the same direction as the actuator. This node acted to shorten the spring, increasing the natural frequency of the system in Fig. 3(b) and thereby moving the zero pair to higher frequency. The movement of this node toward the agonist actuator as the decoupling gain went to zero shows that the dedicated case is a limiting form of the decoupled case.

Jacobsen *et al.* [25] applied the dedicated approach described in this brief but did not describe the frequency response or the origins of their system's dynamics. Potkonjak *et al.* [28] decoupled an AA system to remove interactions, but focused more on the switching of AA roles and closed loop performance than the origins of the open-loop frequency response. Palli *et al.* [26] and Sardelletti *et al.* [27] applied a decoupled approach in a robotics application. Both authors included joint stiffness as one of the control tasks. Joint stiffness is of interest in robotics where the robot's interaction with the environment is important, an issue so far not considered with JMSs. In both robotics applications, the frequency response was still not described.

The system dominated by low-frequency pole and zero pairs also includes a mid-range zero pair that interferes with accurate tension measurements. The mid-range zero pair appeared at the natural frequency of the subsystem defined by the load cell mass and the antagonist stiffness, the impedance of this subsystem was zero and no force was needed across the load cell's stiffness to make it translate with the antagonist actuator. The elbow mass no longer had an effect because its inertia essentially made it a rigid support at this frequency. This zero pair appeared in the measured tension transfer function only and thus limited system performance because it manifested as an error in tendon tension measurement. The applied tension transfer function showed no mid-range zeros, so although no tendon tension was measured, a force was applied to the elbow at that zero pair's frequency. Similar problems have arisen in robotic force control problems. Eppinger and Seering [31] and Colgate and Hogan [32] described instabilities arising from the separation of force application and force measurement.

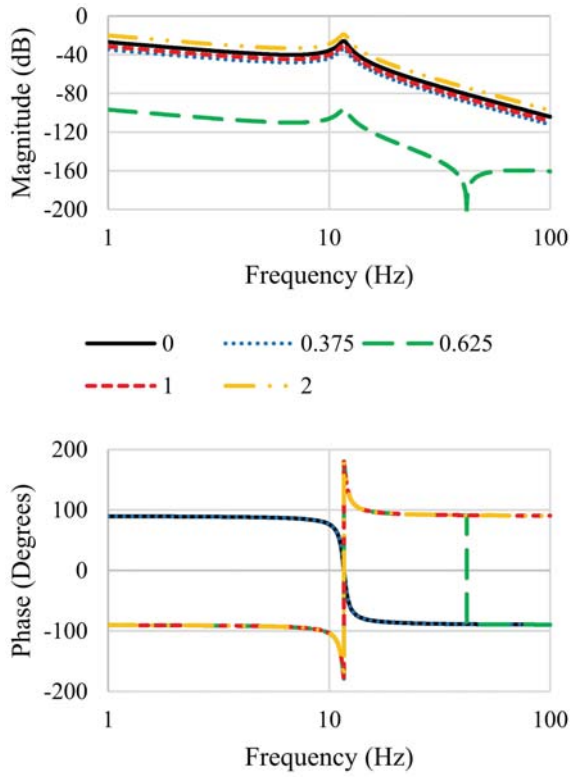

Fig. 7. Joint position frequency response due to tension control as a function of different decoupling gains. For the given system, perfect decoupling of tendon tension control from joint position occurs for a decoupling gain of approximately 0.625. As decoupling gains approach this ideal value from above or below, the magnitude of joint motion due to tension control drops.

A similar problem arose in the current research because the separation between the locations of tension measurement and of the tension application. This separation created the possibility of overcompensation by a controller functioning on an underestimate (measured tension) of the applied tension.

The transfer functions from tension control signal to elbow position showed that the decoupled controller's low-frequency gain was dictated by the decoupling gain (Fig. 7). As the stiffness difference on either side of the mass increased, the decoupling gain slowed the velocity input to a stiffer side or sped up the velocity input to a more compliant side in order to maintain the same force application to each side of the elbow mass. The decoupled controller thereby prevented elbow movement due to tension control action, which the dedicated case could not do. Reduction of interaction in the dedicated case was possible only through the increase of the agonist stiffness. With higher agonist stiffness, changes in antagonist tension due to tendon tension control caused less displacement of the mass. This approach, however, is ineffective in cases where AA roles switch throughout a trial [25], [28], [30].

The AA system can also be viewed as the combination of two serial elastic actuators (SEAs) as described by Pratt and Williamson [33]. Pratt and Williamson's SEAs provide more stable force control than a stiffer system, but come with the drawback of larger actuator displacements. Similarly, more antagonist compliance makes antagonist tension control more stable, but also hinders elbow position control because the elbow's natural frequency drops and a given change in force applied to the elbow requires a greater actuator movement.

This brief studied open loop, tendon tension control dynamics as a means to understand the fundamental limitations encountered in JMS control. Joint position control was included only insofar as position was disturbed by tendon tension control. Additional analysis of the two methods applied to joint position control would make their benefits and drawbacks clearer. Additionally, the system was only studied for FE at one angle. Although testing at numerous angles in both FE and PS would go further to validate the model, the quality of the agreement between model and identification demonstrates the model's usefulness. A nonlinear approach or the inclusion of additional dynamics, such as the drive and motor dynamics, may add accuracy to the model's behavior, but reduce clarity in the sources of the dynamics.

VI. Conclusion

Through a comparison of open-loop dynamics, this brief showed a decoupled approach to tendon tension control of a joint motion simulator's AA actuator pair was superior to a dedicated approach. The decoupled approach controlled tendon tension over a larger bandwidth and interacted less with joint position control. The sources of the open-loop dynamics were explained through models validated with the frequency domain identification of an elbow JMS's FE DOF.

References

[1] J. A. Johnson, D. A. Rath, C. E. Dunning, S. E. Roth, and G. J. W. King, "Simulation of elbow and forearm motion *in vitro* using a load controlled testing apparatus," *J. Biomech.*, vol. 33, no. 5, pp. 635–639, 2000.

[2] C. E. Dunning, K. D. Gordon, G. J. W. King, and J. A. Johnson, "Development of a motion-controlled *in vitro* elbow testing system," *J. Orthopaedic Res.*, vol. 21, no. 3, pp. 405–411, 2003.

[3] J.-R. Haugstvedt, L. J. Berglund, P. G. Neale, and R. A. Berger, "A dynamic simulator to evaluate distal radio-ulnar joint kinematics," *J. Biomech.*, vol. 34, no. 3, pp. 335–339, 2001.

[4] L. Kuxhaus, P. J. Schimoler, J. S. Vipperman, and M. C. Miller, "Validation of a feedback-controlled elbow simulator design: Elbow muscle moment arm measurement," *J. Med. Devices*, vol. 3, no. 3, p. 031002, 2009.

[5] S. Erhart, M. Lutz, R. Arora, and W. Schmoelz, "Measurement of intraarticular wrist joint biomechanics with a force controlled system," *Med. Eng. Phys.*, vol. 34, no. 7, pp. 900–905, 2012.

[6] F. W. Werner *et al.*, "Wrist joint motion simulator," *J. Orthopaedic Res.*, vol. 14, no. 4, pp. 639–646, 1996.

[7] R. E. Debski, P. J. McMahon, W. O. Thompson, S. L.-Y. Woo, J. J. P. Warner, and F. H. Fu, "A new dynamic testing apparatus to study glenohumeral joint motion," *J. Biomech.*, vol. 28, no. 7, pp. 869–874, 1995.

[8] H. B. Henninger, A. Barg, A. E. Anderson, K. N. Bachus, R. Z. Tashjian, and R. T. Burks, "Effect of deltoid tension and humeral version in reverse total shoulder arthroplasty: A biomechanical study," *J. Shoulder Elbow Surgery*, vol. 21, no. 4, pp. 483–490, 2012.

[9] A. E. Kedgley *et al.*, "The effect of muscle loading on the kinematics of *in vitro* glenohumeral abduction," *J. Biomech.*, vol. 40, no. 13, pp. 2953–2960, 2007.

[10] L. Sins, P. Tétreault, Y. Petit, N. Nuño, F. Billuart, and N. Hagemeister, "Effect of glenoid implant design on glenohumeral stability: An experimental study," *Clin. Biomech.*, vol. 27, no. 8, pp. 782–788, 2012.

[11] N. Wuelker, C. J. Wirth, W. Plitz, and B. Roetman, "A dynamic shoulder model: Reliability testing and muscle force study," *J. Biomech.*, vol. 28, no. 5, pp. 489–491 and 493–499, 1995.

[12] J. Burg, K. Peeters, T. Natsakis, G. Dereymaeker, J. V. Sloten, and I. Jonkers, "*In vitro* analysis of muscle activity illustrates mediolateral decoupling of hind and mid foot bone motion," *Gait Posture*, vol. 38, no. 1, pp. 56–61, 2013.

[13] M. L. Hansen, J. C. Otis, S. M. Kenneally, and J. T. Deland, "A closed-loop cadaveric foot and ankle loading model," *J. Biomech.*, vol. 34, no. 4, pp. 551–555, 2001.

[14] L. D. Noble, R. W. Colbrunn, D.-G. Lee, A. J. van den Bogert, and B. L. Davis, "Design and validation of a general purpose robotic testing system for musculoskeletal applications," *J. Biomech. Eng.*, vol. 132, no. 2, p. 025001, 2010.

[15] K.-J. Kim *et al.*, "*In vitro* simulation of the stance phase in human gait," *J. Musculoskeletal Res.*, vol. 5, no. 2, pp. 113–121, 2001.

[16] C. Nester *et al.*, "*In vitro* study of foot kinematics using a dynamic walking cadaver model," *J. Biomech.*, vol. 40, no. 9, pp. 1927–1937, 2007.

[17] N. A. Sharkey and A. J. Hamel, "A dynamic cadaver model of the stance phase of gait: Performance characteristics and kinetic validation," *Clin. Biomech.*, vol. 13, no. 6, pp. 420–433, 1998.

[18] M. C. Anderson, N. A. Brown, K. N. Bachus, and B. A. MacWilliams, "A cadaver knee simulator to evaluate the biomechanics of rectus femoris transfer," *Gait Posture*, vol. 30, no. 1, pp. 87–92, 2009.

[19] J. M. Bach and M. L. Hull, "A new load application system for *in vitro* study of ligamentous injuries to the human knee joint," *J. Biomechan. Eng.*, vol. 117, no. 4, pp. 373–382, 1995.

[20] J. Hashemi, N. Chandrashekar, T. Jang, F. Karpat, M. Oseto, and S. Ekwaro-Osire, "An alternative mechanism of non-contact anterior cruciate ligament injury during jump-landing: *In-vitro* simulation," *Experim. Mech.*, vol. 47, no. 3, pp. 347–354, 2007.

[21] L. P. Maletsky and B. M. Hillberry, "Simulating dynamic activities using a five-axis knee simulator," *J. Biomech. Eng.*, vol. 127, no. 1, pp. 123–133, 2005.

[22] C. A. McLean and A. M. Ahmed, "Design and development of an unconstrained dynamic knee simulator," *J. Biomech. Eng.*, vol. 115, no. 2, pp. 144–148, 1993.

[23] A. H. Hoskins, A. R. Fauth, and N. A. Sharkey, "Dynamic cadaveric gait simulation: Steps into the future," presented at the 28th Annu. Meet. Amer. Soc. Biomech., Portland, OR, USA, 2004.

[24] L. M. Ferreira, "Development of an active elbow motion simulator and coordinate systems to evaluate kinematics in multiple positions," Ph.D. dissertation, Dept. Biomed. Eng., Univ. Western Ontario, London, ON, Canada, 2011, paper 84.

[25] S. C. Jacobsen, H. Ko, E. K. Iversen, and C. C. Davis, "Antagonistic control of a tendon driven manipulator," in *Proc. IEEE Int. Conf. Robot. Autom.*, May 1989, pp. 1334–1339.

[26] G. Palli, C. Melchiorri, T. Wimböck, M. Grebenstein, and G. Hirzinger, "Feedback linearization and simultaneous stiffness-position control of robots with antagonistic actuated joints," in *Proc. IEEE Int. Conf. Robot. Autom.*, Apr. 2007, pp. 4367–4372.

[27] I. Sardellitti, G. Palli, N. G. Tsagarakis, and D. G. Caldwell, "Antagonistically actuated compliant joint: Torque and stiffness control," in *Proc. IEEE/RSJ Int. Conf. Intell. Robots Syst. (IROS)*, Oct. 2010, pp. 1909–1914.

[28] V. Potkonjak, B. Svetozarevic, K. Jovanovic, and O. Holland, "The puller-follower control of compliant and noncompliant antagonistic tendon drives in robotic systems," *Int. J. Adv. Robot. Syst.*, vol. 8, no. 5, pp. 143–155, 2011.

[29] S. Skogestad and I. Postlethwaite, *Multivariable Feedback Control: Analysis and Design*, vol. 2. New York, NY, USA: Wiley, 2007.

[30] P. J. Schimoler, J. S. Vipperman, and M. C. Miller, "Hierarchical control improves joint motion simulator performance," presented at the 39th Annu. Meet. Amer. Soc. Biomech., Columbus, OH, USA, 2015.

[31] S. D. Eppinger and W. P. Seering, "Three dynamic problems in robot force control," in *Proc. IEEE Int. Conf. Robot. Autom.*, May 1989, pp. 392–397.

[32] E. Colgate and N. Hogan, "An analysis of contact instability in terms of passive physical equivalents," in *Proc. IEEE Int. Conf. Robot. Autom.*, May 1989, pp. 404–409.

[33] G. A. Pratt and M. M. Williamson, "Series elastic actuators," in *Proc. IEEE/RSJ Int. Conf. Intell. Robots Syst. Hum. Robot Interact. Cooper. Robots*, Aug. 1995, pp. 399–406.